Analyst

PAPER

View Article Online
View Journal | View Issue

Cite this: *Analyst*, 2014, **139**, 1134

Impedance nanopore biosensor: influence of pore dimensions on biosensing performance

Krishna Kant,[ac] Jingxian Yu,[b] Craig Priest,[d] Joe G. Shapter[a] and Dusan Losic*[c]

Received 12th October 2013
Accepted 28th December 2013

DOI: 10.1039/c3an01933k

www.rsc.org/analyst

Knowledge about electrochemical and electrical properties of nanopore structures and the influence of pore dimensions on these properties is important for the development of nanopore biosensing devices. The aim of this study was to explore the influence of nanopore dimensions (diameter and length) on biosensing performance using non-faradic electrochemical impedance spectroscopy (EIS). Nanoporous alumina membranes (NPAMs) prepared by self-ordered electrochemical anodization of aluminium were used as model nanopore sensing platforms. NPAMs with different pore diameters (25–65 nm) and lengths (4–18 μm) were prepared and the internal pore surface chemistry was modified by covalently attaching streptavidin and biotin. The performance of this antibody nanopore biosensing platform was evaluated using various concentrations of biotin as a model analyte. EIS measurements of pore resistivity and conductivity were carried out for pores with different diameters and lengths. The results showed that smaller pore dimensions of 25 nm and pore lengths up to 10 μm provide better biosensing performance.

1 Introduction

Integration of biomolecules into nanopores and nanochannels has attracted considerable attention due to the high surface area of the pores and similarity with nanopores in biological systems meaning there is the potential for new and advanced biosensing devices.[1–3] In these studies specific recognition molecules have been functionalized inside single or nanopore arrays for various applications including molecular or ionic gates, single molecule detection, and biosensing of enzymes DNA and antibodies.[4,5] Development of nanochannel or nanopore array biosensing devices has proven to be an excellent approach toward the development of simple, inexpensive and highly sensitive biomolecule detection. The sensitivity, low cost, simplicity, and easy miniaturization of electrochemical detection is particularly suited to the development of highly sensitive nanopore based biosensors. However, to improve and optimize the performance of nanopore biosensors, it is essential to understand the electrical and electrochemical properties of the nanopores, the dependence of these properties on nanopore dimensions, the diffusion and molecular transport of analyte molecules inside the nanopores, and their physical and chemical interactions. In particular, their interactions and specific binding with the immobilized probe confined in a nanoscale volume are critical parameters which determine the performance of biosensing devices, *e.g.* sensitivity, response time and detection limit.[6,7] Surprisingly there are only few electrochemical studies on nanopores that address these questions.[8,9]

Electrochemical impedance spectroscopy (EIS) is a powerful method for analysing the complex electrochemical properties of a system and possible changes of its bulk properties. Therefore, it has been widely used for characterization of charge transport across nanopores in membranes and membrane/solution interfaces.[10,11] EIS is also very powerful and sensitive for the detection of antigen–antibody binding inside nanopores.[12,13] Impedance biosensing can be performed using both faradaic and non-faradaic processes. In faradaic processes charge is flowing across the interface of the sensing material; however in the case of non-faradic sensing, current flows without charge transfer through the interface material. The main disadvantage of the faradic process is that it requires a redox species to enhance the signal of the electron transfer. On the other hand, there are no additional requirements of a redox species or signal enhancer for non-faradaic EIS. Hence, in the field of nanopore biosensors the non-faradic EIS is particularly well-suited for the detection of binding events inside nanopores and is recognized as the simpler method.[2,14]

Nanoporous alumina membranes (NPAMs) prepared by electrochemical anodization process have been very attractive for development of nanopore biosensing devices, due to their uniform pore size, high aspect ratio, high surface area and straight-forward and inexpensive fabrication.[15] It has been demonstrated that the electron transfer resistance will decrease

[a]*School of Chemical and Physical Sciences, Flinders University, Bedford Park, Adelaide 5042, Australia*

[b]*School of Chemistry and Physics, The University of Adelaide, AdelaideSA 5005, Australia*

[c]*School of Chemical Engineering, The University of Adelaide, Adelaide, SA5005, Australia. E-mail: Dusan.losic@adelaide.edu.au; Tel: +61 8 8013 4648*

[d]*Ian Wark Research Institute, University of South Australia, Mawson Lakes, Adelaide 5095, Australia*

and the conductance will increase as a result of a binding reaction inside the pores of NPAM.[16,17] However, the binding reaction of the antigen at the antibody-immobilized surface is often insufficient to produce a large signal change for impedance measurements that are largely dependent of nanopore dimensions and the density of immobilized probes inside nanopores.[18–20] Previous studies demonstrated that the transport of ions or molecules passing through bio-functionalized nanopores is affected by steric and electrostatic effects.[21–23] The electrostatic effect is a long-range effect caused by the interaction between surface-immobilized charged molecules and the transporting ions.[8,16,23] This transport is shown to be dependent on pore size and number of pores and can be changed by the surface charge or ionic strength of the bulk solution, which can also change ion transport inside the nanopores.[5,24,25] These studies clearly demonstrate the need for a detailed investigation of the influence of nanopore dimensions on their electrochemical properties and biosensing performance.

Herein the EIS electrochemical method was used to study the effect of nanopore diameters and length on the performance a label-free nanopore biosensor. The NPAM was used as sensing nanopore platform and biotin–streptavidin detection was used as a model of immune assay biosensor. The aim was to demonstrate the application of a NPAM array as simple, low cost and label-free electrochemical biosensing platform for detection of biomolecules based on affinity binding reactions. The scheme of the proposed biosensing device and the experimental setup is shown in Fig 1. The NPAM sensing platforms with different diameters and length of the nanopores were prepared to characterize their electrochemical properties and biosensing performance using various concentrations of analytes.[6,26,27] The surface inside the pores was functionalized by phosphonic acid and NHS–EDC chemistry, followed by the covalent attachment of antibody molecules, which were used as a binding surface for the selective capture of antigen molecules, *i.e.* biotin.[28] The NPAM sensing platform with a reduced number of nanopores and working area of 20 × 20 μm^2 was prepared by photolithography in order to miniaturize the device. A four electrode cell was used to characterize the change in properties of the nanopore array using EIS technique for different pore diameter and length.

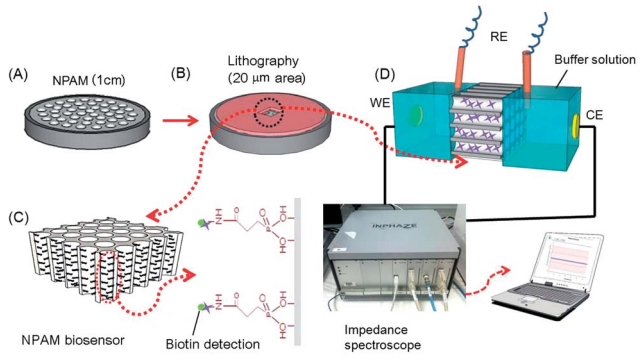

Fig. 1 A schematic of experimental setup (a) fabricated nano porous alumina membrane (NPAM) (b) NPAM after photolithography with a 20 × 20 μm^2 opening (c) NPAM modified with streptavidin as sensing platform (d) NPAM placed in EIS cell for impedance characterization.

2 Experimental

2.1. Preparation of nanoporous alumina membranes (NPAM)

Nanoporous alumina membranes (NPAMs) were prepared by a two-step anodization process using 0.3 M oxalic acid as the electrolyte at 0 °C as described elsewhere.[9,29] The first anodized porous layer was prepared at a voltage of 60 to 80 V for 5 min, and then removed using an oxide removal solution (0.2 M chromium trioxide and 0.4 M phosphoric acid) for 1–2 hours at 60 °C. The second anodization was carried out in a range of 30 V to 70 V to achieve different pore diameters. Mild anodization at 30 V was used to get small pore diameters of 25 ± 5 nm while hard anodization at 70 V for large pore diameters of 65 ± 5 nm. The pore length in a NAPM is controlled by the time duration of anodization. For mild anodization at 30 V and 180 min was used to achieve pore length about 4–5 μm. However for hard anodization at 70 V it took only 20 min to grow 4–5 μm long pores.

To prepare NPAMs with different thicknesses or lengths of small diameter pores the anodization time was varied from 180 min to 720 min at 30 V. Once the anodization completed the remaining aluminium was removed from the backside of the nanopore array to reveal a clear and clean barrier layer of the nanopore array by using $CuCl_2$/HCl. The removal of barrier layer from the pore structures was performed by using the 10% phosphoric acid for 2 hours.

2.2. Photolithography on NPAM

The fabricated NPAM was patterned on the back side with photoresist using photolithography to prepare a 20 μm × 20 μm area with the opened nanopore array. The photoresist (AZ1518) was spin-coated (1500 rpm) over the bottom side of NPAM (barrier layer) and followed by baking of the sample at 100 °C for 50 s. A photo-mask (chrome-on-glass mask, Bandwidth Foundry) with a 20 μm diameter transparent region was used to mask the sample with exposure of 330 mJ m^{-2}. The exposed photoresist was then removed by solvent. In this way an opening of a 20 μm square on the NPAM from bottom side was obtained.

2.3. Functionalization of NPAM nanopores with streptavidin

Surface modification of NPAM nanopore array was performed by soaking in an aqueous solution of 5 mM 2-carboxyethyl phosphonic acid for 72 hours at room temperature. The samples were rinsed with a sufficient amount of DI water and then dried under a slow purge of nitrogen. The top and bottom surfaces of the nanopore array were exposed to air plasma etching for 30 seconds, using a plasma cleaner (Diener, Germany). After exposing the nanopore array to plasma etching, the samples were left in DI water for 24 hours at room temperature for pore wetting. After pore wetting the nanopore array was soaked in *N*-hydroxysuccinimide (NHS) 15 mg mL^{-1} in PBS and 1-ethyl-3-(3-dimethylaminopropyl) carbodimide (EDC) 20 mg mL^{-1} in PBS buffer solution for 30 min at room temperature,

followed by rinsing with plenty of DI water. Subsequently the samples were soaked in streptavidin solution of 100 μg mL^{-1} concentration in PBS for 30 min at room temperature to functionalize the nanopores. The samples of prepared NPAM biosensing platform were finally washed in copious amounts of DI water and mounted in the electrode cell for EIS study of reaction with different concentration of biotin. The biotin stock solution of 50 μg mL^{-1} was prepared and used to make required concentrations (0.2 μM to 29 μM) by dilution. The prepared biotin solution were injected with the same volume on the streptavidin functionalized NPAM sensor and left for the reaction time of 15 min to complete binding reaction followed by washing with DI water and EIS measurements.

2.4. Electrochemical measurements

Electrochemical measurements were carried out in using an EIS spectrometer, (Inphaze Pty. Ltd. Sydney, Australia) with a four-electrode system which is specifically designed for EIS characterization of NPAM.[30] Two gold foils formed the working and counter electrodes with two Ag/AgCl as reference electrodes. The nanoporous array was sandwiched between two cell chambers filled with the buffer solution in contact with reference electrodes on each side. The working and counter electrodes were respectively placed at the end of two chambers (Fig 1). An equivalent circuit (Fig. 5) is used to balance the resistance and capacitance for the entire system and monitor the behavior of nanoporous arrays and changes on their surface. Since the streptavidin molecules can be negatively or positively charged depending on environment, an electric double layer is expected to be present at the streptavidin-solution interface. An impedance contribution from this interface is represented as a parallel RC element (R_{Fn} and C_{Fn}), and commonly introduced in series with the nanopore resistence.[31,32] Here, R_{sol} is resistance of the electrolyte solution, R_p and C_p are the total contribution of resistance and capacitance of alumina membranes and free nanopores, R_{Fn} and C_{Fn} are the resistance and capacitance of the electric double layer formed at interface between the protein molecules and the solution. This simplified electrical model provides the best fit to our measurements. Particularly, a similar equivalent circuit is adopted to investigate glass nanopores in aqueous solutions.[33] This model assumes that there is no impedance contribution made from the limited diffusion of the ions. In practice, such contribution does exist but mainly influences the impedance characteristics within a very low frequency range.[13,34] However, for our purposes the proposed model is sufficient, as we are able to extract the relevant model parameters, such as R_p, R_{Fn}, which are not affected by the limited diffusion. The resistance of the area of membrane, which is covered with photoresist, is so high that it does not appear in the equivalent circuit model presented. Theoretically the pore resistance R_p can be calculated as:

$$R_p = \frac{4L}{\pi\sigma d^2}$$

where R_p is pore resistance, L is length of the pore and d is the diameter of the pore.[35] As we increase the diameter of the pore the value of pore resistance reduces but at the same time it increase if we vary the length of the nanopore array. The biotin solutions of 0.2–29 μM concentrations in buffer 7.4 pH were tested in a series of experiments to explore their binding with functionalized streptavidin molecules inside the NPAM arrays. The electrochemical impedance measurements were acquired for each biotin concentration separately in the frequency range from 1 Hz to 1 MHz. A minimum of 3 spectra was taken for each concentration of the biotin and 3–4 samples was used.

3 Results and discussion

The morphological change in NPAM leads to change in the sensing capability of biosensing device. To optimize these parameters a number of experiments with different morphologies were undertaken and are discussed in the following section.

3.1. SEM characterization of fabricated NPAMs

SEM images of the top surface of the prepared NPAM sensing platform with different pore diameter are presented in Fig 2(a)–(d). The images confirm the successful preparation of well-ordered nanopores with a diameter of 25 ± 2 nm, 45 ± 2 nm and 65 ± 2 nm depending on the anodization conditions. To achieve three different pore diameters at constant pore length the anodization potential was tuned between 30–70 V with the anodization time varied from 20–180 min.

It is well known that pore diameter is determined by applied voltage during anodization and that the porosity (P) of the NPAM can be estimated assuming an ideal hexagonal arrangement of the pores;

$$P = \left(\frac{\pi}{2\sqrt{3}}\right)\left(\frac{D_p}{D_{int}}\right)^2$$

where D_p and D_{int} are pore diameter and the inter-pore distance respectively.[36] A typical cross-sectional structure of the prepared NPAM is shown in Fig 2(d), with the inset figure (scale bar 100 nm) showing well-ordered and aligned pores through the full thickness of the membrane. The pore length was calibrated against anodization time (2–10 h) for the 25 nm diameter pores, to allow the NPAM pore length, which is equal to the thickness of the NPAM, to be tuned. In Fig 2(e), the calibration data is plotted for four different pore lengths from 5 μm to 20 μm at constant anodization potential 40 V.[26,37] The linear fit to the calibration data is very good, providing excellent control over the pore length for this study.

3.2. Surface modification and characterization of NPAMs

FTIR spectra of control NPAM and modified NPAM with phosphonic acid (PHA) are shown in Fig 2(f). The results show evidence of surface modification of NPAM by immobilization of biosensing molecules inside the nanopores. The peaks observed at 1450 cm^{-1} and 1485 to 1580 cm^{-1} are associated with available (COO^-) group which will lead to further bonding of protein molecules. The peaks at 2500 cm^{-1} to 2650 cm^{-1} show the presence of P–OH and P–H bonding and the peaks at

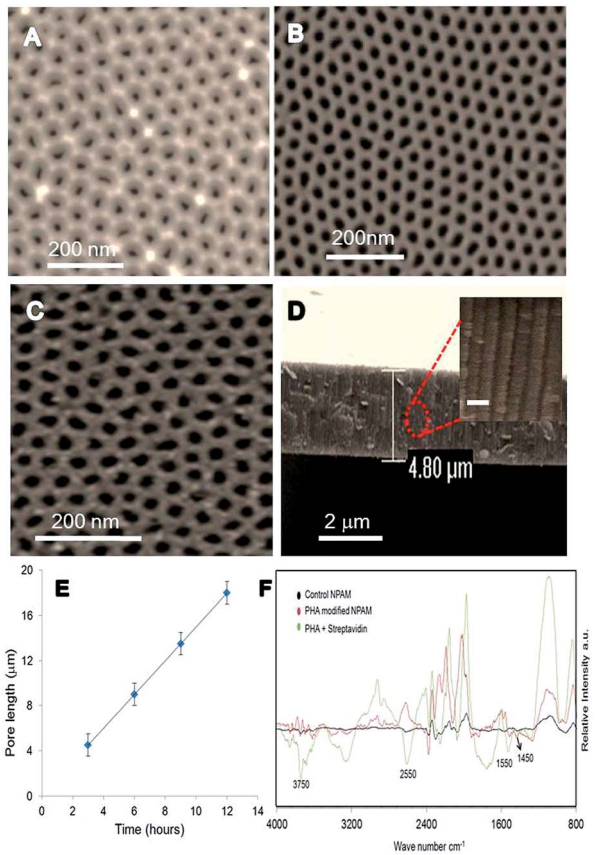

Fig. 2 SEM images of the top surface of NPAM used as nanopore sensing with different pore diameters (a) small pore around 25 ± 2 nm (b) medium size pore around 45 ± 2 nm (c) large pore around 65 + 2 nm, which are prepared in 0.3 M oxalic acid electrolyte using different anodization voltages 30–70 V and times from 20 to 180 min to achieve the same pore length (d) cross section SEM images of NPAM with magnified view of nanopores (100 nm scale) (e) calibration graph showing fabrication of NPAM with the different pore length using anodization time from 3–12 hours (f) FTIR spectra of NPAM before and after the first step of surface modification with phosphonic acid.

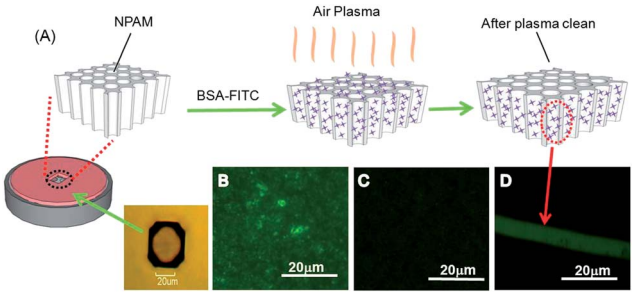

Fig. 3 Schematic of surface modification of NPAM nanopores to demonstrate functionalization of only internal pore structures and the clean top surface obtained using an air plasma process. A fluorescent labelled albumin bovine serum BSA-FITS are used as a model molecule. (a) NPAM surface modification with phosphonic acid and covalently attached BSA-FITS followed by air plasma treatment. (b) Fluorescent image of NPAM before and (c) after plasma treatment (d) cross section image of NPAM which proof that surface modification is still inside the pores after air plasma treatment.

3650 to 3750 cm^{-1} represent the free OH groups available at the surface of the NPAM.[38]

To achieve selective immobilization of the probe biomolecule (streptavidin) inside the nanopores, we developed a surface functionalization procedure, which involves modification of NPAM with phosphonic acid (PHA), activation of COOH with *N*-hydroxysuccinimide–1-ethyl-3-(3-dimethylaminopropyl) carbodiimide (NHS–EDC) and covalent binding of streptavidin–biotin. The most critical part of this process was to ensure that biologically active probes were exclusively inside the nanopores, *i.e.* that the top (outer) surface of the NPAM was unmodified. Therefore, we used air plasma to clean the outer surface before and after NHS–EDC activation. This process is schematically represented in Fig 3a. To demonstrate that functional groups remain only inside the nanopores, fluorescence images of the top (outer) surface and the cross-section of the NPAM were collected after treatment with BSA-FITC and plasma, see fluorescence image from the top surface (Fig 3b) before plasma treatment clearly shows the bright fluorescence of the BSA-FITC image, confirming the presence of BSA on the top surface. The image in Fig 3c is the same top surface after plasma treatment and shows negligible fluorescence intensity, confirming that the removal of active biomolecules from the top surface of the NPAM was successful. Furthermore, the cross-section image of the NPAM (Fig 3d) clearly shows that the fluorescence signal remains inside nanopores, demonstrating that our method can achieve a highly selective surface modification inside the nanopores. The amino groups after NHS–EDC modification are active inside the nanopores for binding of streptavidin molecules and, therefore, the approach is suited to the preparation of a nanopore biosensing device.

3.3. EIS measurements of NPAM biosensor

In order to characterize the label-free sensing performance of these NPAM biosensors and optimization of the nanopore dimensions for sensing protein molecules, a series of electrochemical impedance measurements were carried out. In the first set of experiments, NPAM biosensors with three different average pore diameters (25, 45, and 65 nm) were characterized using biotin analytes with concentrations from 0.2 μM to 29 μM. The collected impedance (Z) data as a Nyquist plot for the different pore diameters using a fixed concentration of biotin (0.2 μM) are shown in Fig. 4(a) to reveal the frequency dependence on the pore diameter. The graphs show that Z decreased with increasing NPAM pore size.

To estimate the pore resistance, we modelled the experimental system using EvolCRT software[39] (developed by Department of Chemistry, Wuhan University, China) according to the equivalent circuit (Fig. 5a inset). The simulation of the data was done using the following equation:

$$F = \frac{1}{N}\sum_{i=1}^{m}\left[\left(\tilde{Z}_i' - Z_i'\right)^2 + \left(\tilde{Z}_i'' - Z_i''\right)^2\right]$$

where Z_i' and Z_i'' are the experimental values of the real part and the imaginary part of the electrochemical impedance at a given frequency f_i. Similarly $\tilde{Z}_i'$ and $\tilde{Z}_i''$ are the corresponding fitting

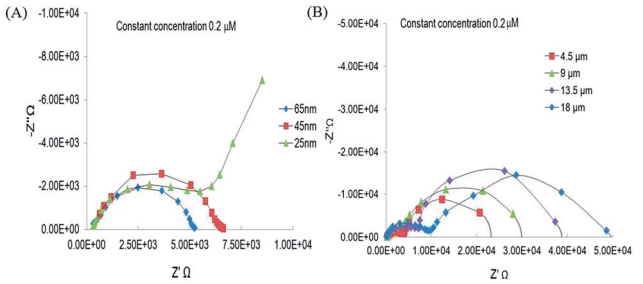

Fig. 4 (a) Nyquist plot obtained for NPAM biosensors with different pore diameters of NPAM and (b) different pore length at constant pore diameter and their response using constant biotin concentration (0.2 μM).

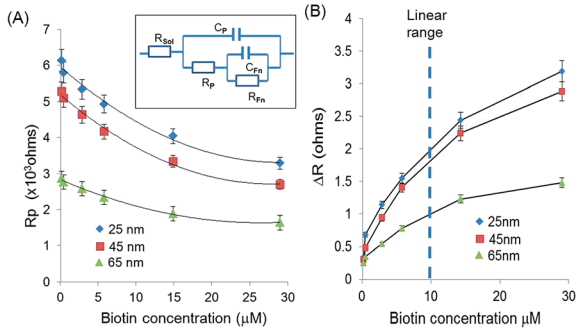

Fig. 5 (a) A plot showing relation between the pore diameter and biotin concentration and their influence on the nanopore resistance R_p. The proposed equivalent circuit (inset) used for the simulation of experimental data is presented. (b) Calibration graph showing changes of pore resistance ΔR with biotin concentration using NPAM biosensor with different pore diameter.

values. Here m is the number of input frequencies, *i.e.* the number of data points. The extracted parameters of the proposed equivalent circuit are as follow in table 1:

The best fit for the pore resistance (R_p) was obtained from these simulations at several concentrations of biotin and three different pore diameters. The experimental data was simulated against the equivalent circuit to determine the exact value for the pore resistance. The R_p is a key parameter related to changes inside the nanopore because the active binding sites for the analyte are only available inside the nanopore. The values for R_p obtained after simulation with equivalent circuit and plotted in Fig. 5a, showing the influence of pore diameter and biotin concentration on R_p. At the lowest concentration of biotin 0.2 μM, the pore resistance decreases from 6.1×10^3 to 2.8×10^3 Ω when the pore diameter is increased from 25 to 65 nm showing better sensitivity using NPAM platform with smaller nanopores.

To explain observed behaviour it is important to consider other parameters including not only pore diameters but also the size and charge of analyte molecules and charge of immobilized molecules inside nanopores (streptavidin). The molecular size of streptavidin tetramer is about 4–5 nm and it is immobilized as a monolayer inside pores, and its molecular size increased around 6–8 nm after the binding of biotin. This binding reaction causes a significant change of surface charge and conductivity of formed streptavidin–biotin complex and consequently pore resistance, which is used as a parameter for impedance biosensing. These resistance/conductivity changes from binding reaction inside smaller nanopore (<25 nm) are more significant because charged analyte molecules are very close to each other and more sensitive to AC oscillation of ions inside the nanopore compared to large nanopores. In the case of large pore diameter (65 nm) the intermolecular interaction as result of binding of analyte molecules (biotin) is less influential and the impedance measurement is dominated by the bulk properties of the solution (as there is enough space inside the pores) and small changes in impedance due to effects at the walls of the nanopores become insignificant. So it can be concluded that the molecular size of biotin and streptavidin don't have significant effect for larger pore diameters. This type of nanopore biosensing concept based on changing conductivity without of the use of pore blocking mechanism is previously demonstrated for impedance biosensing of DNA hybridization.[28,40] For this type of nanopore biosensors having the smaller pores is beneficial because the influence of the surface effects is greater and the signal is affected significantly (lesser area available for bulk solution) as reported in previous studies.[41,42] However, there is limitation, if the pore diameters are reduced below 10 nm we may observe high pore resistance due to the limited transport of biomolecules inside the nanopores, which could block nanopores at some point of concentration.

The resistivity change $\Delta R = R_0 - R_x$ is presented as a biosensing signal where R_0 is value taken with pore resistance at zero biotin concentration and R_x taken for pore resistance on each biotin concentration (Fig. 5b). It was observed that the increase in ΔR value is linear at lower concentration range and at concentrations over 10 μM the graph tends to reach saturation phase. Interestingly this behaviour is observed for both small and large nanopores and it is not influenced by the pore diameters. This result suggests that saturation signal is related to the surface reaction and binding all available streptavidin molecules (Fig. 5b).

Since it was found that the smaller pore diameter provides greater sensitivity and performance, we used the NPAM platform with 25 nm pore diameters to study the influence of pore length on electrochemical signal and biosensing performance.

Table 1 The extracted value for all the components of equivalent circuit for different nanopore diameter and length

	R_{sol} (Ω)	R_p (Ω)	R_{Fn} (Ω)	C_p (F)	C_{Fn} (F)
Pore diameter (nm)					
65	5.87×10^2	3.07×10^3	1.81×10^3	1.54×10^{-9}	6.68×10^{-9}
45	6.35×10^2	5.35×10^3	5.43×10^3	3.29×10^{-9}	6.10×10^{-8}
25	6.02×10^2	6.16×10^3	1.8×10^4	3.68×10^{-9}	2.47×10^{-9}
Pore length (μm)					
4.5	6.46×10^2	6.41×10^3	1.79×10^4	4.50×10^{-9}	4.43×10^{-7}
9	6.39×10^2	7.54×10^3	2.26×10^4	1.58×10^{-8}	9.86×10^{-8}
13.5	6.79×10^2	8.25×10^3	2.98×10^4	3.53×10^{-9}	1.97×10^{-7}
18	6.94×10^2	1.61×10^4	3.34×10^4	4.47×10^{-9}	1.70×10^{-6}

For that purpose we fabricated NPAM biosensing platforms with different pore lengths (4.5 μm, 9 μm, 13.5 μm and 18 μm) and carried out a series of EIS measurements at different concentrations of biotin. The Nyquist plot was generated from a constant concentration of biotin (0.2 μM) as shown on Fig. 4b. The graph shows the trend of increasing impedance over the range of frequencies with respect to increasing pore length. Further measurements were performed by simulating the experimental data with the proposed equivalent circuit to find value of R_p for various length of NPAM (Fig. 6a). It was found that the R_p changed from 3×10^4 to 10.5×10^4 Ω as length of NPAM increased from 4.5 μm to 18 μm. The graph clearly shows the increase in the pore resistance with increasing the pore length. The characteristic saturation in signal was observed at higher concentration of biotin (near 15 μM) showing the upper limit of detection for biotin.

At lower concentration range a linear response ($R^2 = 0.96$) from 0.2 to 10 μM was determined (Fig. 6b). It was found that increasing pore length beyond 10–15 μm did not provide linear responses. Longer nanopores showed higher resistances, hence small changes inside the nanopores were not detectable, as the pore impedance was dominated by NPAM resistance. Increasing nanopore length to more than 10 to 15 μm does not seem too good for such type of biosensing detection as the longer pore lengths mean long for diffusion times of the analyte molecules and hence high resistance for the system.

It was observed that pore resistance is a key factor to be considered in the optimization of biosensing performance of EIS nanopore based devices. In our case the pore resistance at lower concentration (0.2–10 μM) showed linear relationship ($R^2 = 0.96$) with concentration change. The detection limit for biotin concentration using this system was 0.2 μM. However we believe lower concentrations can be detected by lowering nanopore diameters (<25 nm). Nanopores with a diameter below 20 nm are difficult to make using the anodization conditions used in our experiments (oxalic acid), but the use of other electrolytes (sulphuric acid) can produce such pores. However, there is limitation that these smaller nanopores with a diameter between 5–10 nm may not perform well as non-faradic biosensing devices as the small pore size may limit the diffusion of the larger analyte molecules such as protein and enzymes. The best performance for the biosensing platform was observed with nanopore diameters of 20–40 nm with a length of 4–15 μm. Reduction in nanopore length below 10 μm could reduce robustness of NPAM biosensor device and increasing nanopore diameter will also reduce the sensitivity of the system.

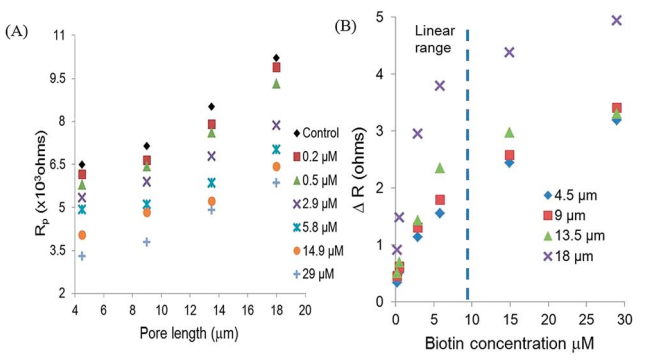

Fig. 6 (a) Graph showing changes of pore resistance ΔR of NPAM biosensor with biotin concentration at different pore length (b) a calibration plot for different pore length of NPAM biosensor at lower concentration (0.2–5.8 μM) of biotin show the significant linearity between actual pore resistance ΔR and biotin concentration.

4 Conclusion

The impact of pore dimensions and surface chemistry of nanopore arrays was explored and their application in a non-faradic impedance nanopore biosensor for the detection of biological entities such as protein molecules was demonstrated. A new method for specific functionalization exclusively inside nanopores was used to achieve the critical effect on electrochemical charge transfer by using nanopore array. The results show that measuring biotin concentrations from 0.2 to 29 μM in PBS buffer solution can be successfully achieved without using any labelled marker or signal enhancer redox probe. It was observed that pore resistance is a key factor to be considered in the optimization of biosensing performance of non-faradic EIS nanopore based devices. The values of R_p show a decrease with the increasing concentration of analyte which is a consequence of the properties of binding biotin molecules inside the nanopores. This behaviour is more significant within the low frequency range 1Hz–20 KHz showing the magnitude of the impedance is affected considerably by the biotin concentration. However, linearity of sensor signal is limited with concentration showing typical saturation at higher concentrations of 30 μM and linear range from 0.2–10 μM. Our results confirmed that pore dimensions including pore diameters and length have considerable influence on biosensing performance. It was found that lowering pore diameters (<30 nm) provides better response and sensitivity. However there is a limitation to the size reduction as sizes comparable to the size of analyte molecules will prevent diffusion molecules inside the pore. Regarding pore length it was found that longer pores (>10 μm) are also not favourable for non-faradic EIS detection due to the higher resistance and long time for diffusion of analyte molecules inside nanopores. Hence it is critical to optimize pore dimensions to achieve optimal performances of nanopore based electrochemical biosensing devices. These devices have considerable potential toward development simple and inexpensive sensing devices for broad biomedical applications.

Acknowledgements

The authors acknowledge the financial support of the Australian Research Council (LP100100272), Flinders University, the University of Adelaide and Industry partner Inphaze Pty. Ltd, Sydney, Australia. Authors acknowledge support of South Australian node of the Australian National Fabrication Facility (ANFF), for the start-up award to use their lithography and clean room facility and Australian Microscopy and Microanalysis Research Facility (AMMRF) for use their facilities at Adelaide Microscopy.

Notes and references

1 B. Y. Chang and S. M. Park, *Annu. Rev. Anal. Chem.*, 2010, **3**, 207–229.
2 J. S. Daniels and N. Pourmand, *Electroanalysis*, 2007, **19**, 1239–1257.
3 O. Pänke, T. Balkenhohl, J. Kafka, D. Schäfer and F. Lisdat, *Biosensing for the 21st Century*, ed. R. Renneberg and F. Lisdat, Springer, Berlin Heidelberg, 2008, vol. 109, ch. 81, pp. 195–237.
4 B. Yameen, M. Ali, R. Neumann, W. Ensinger, W. Knoll and O. Azzaroni, *Nano Lett.*, 2009, **9**, 2788–2793.
5 S. J. Li, J. Li, K. Wang, C. Wang, J. J. Xu, H. Y. Chen, X. H. Xia and Q. Huo, *ACS Nano*, 2010, **4**, 6417–6424.
6 M. Darder, P. Aranda, M. Hernández Vélez, E. Manova and E. Ruiz-Hitzky, *Thin Solid Films*, 2006, **495**, 321–326.
7 E. Reimhult and K. Kumar, *Trends Biotechnol.*, 2008, **26**, 82–89.
8 B. T. T. Nguyen, G. Koh, H. S. Lim, A. J. S. Chua, M. M. L. Ng and C. S. Toh, *Anal. Chem.*, 2009, **81**, 7226–7234.
9 D. Losic, M. Lillo and D. Losic Jr, *Small*, 2009, **5**, 1392–1397.
10 I. F. Cheng, H. L. Yang, C. C. Chung and H. C. Chang, *Analyst*, 2013, **138**, 4656–4662.
11 N. J. Ronkainen, H. B. Halsall and W. R. Heineman, *Chem. Soc. Rev.*, 2010, **39**, 1747–1763.
12 R. Pei, Z. Cheng, E. Wang and X. Yang, *Biosens. Bioelectron.*, 2001, **16**, 355–361.
13 X. Yu, R. Lv, Z. Ma, Z. Liu, Y. Hao, Q. Li and D. Xu, *Analyst*, 2006, **131**, 745–750.
14 J. A. González, V. López, A. Bautista, E. Otero and X. R. Nóvoa, *J. Appl. Electrochem.*, 1999, **29**, 229–238.
15 A. de la Escosura-Muñiz and A. Merkoçi, *Electrochem. Commun.*, 2010, **12**, 859–863.
16 G. Herzog and D. W. M. Arrigan, *Analyst*, 2007, **132**, 615–632.
17 Y. Xiao, C. M. Li and Y. Liu, *Biosens. Bioelectron.*, 2007, **22**, 3161–3166.
18 O. Ouerghi, A. Touhami, N. Jaffrezic Renault, C. Martelet, H. B. Ouada and S. Cosnier, *Bioelectrochemistry*, 2002, **56**, 131–133.
19 E. Dickey, O. Varghese, K. Ong, D. Gong, M. Paulose and C. Grimes, *Sensors*, 2002, **2**, 91–110.
20 P. Takhistov, *Biosens. Bioelectron.*, 2004, **19**, 1445–1456.
21 R. K. Potucek, R. G. Rateick and V. I. Birss, *J. Electrochem. Soc.*, 2006, **153**, B304–B310.
22 B. T. T. Nguyen, A. E. K. Peh, C. Y. L. Chee, K. Fink, V. T. K. Chow, M. M. L. Ng and C.-S. Toh, *Bioelectrochemistry*, 2012, **88**, 15–21.
23 M. E. Orazem and B. Tribollet, *Electrochim. Acta*, 2008, **53**, 7360–7366.
24 F. Eftekhari, C. Escobedo, J. Ferreira, X. Duan, E. M. Girotto, A. G. Brolo, R. Gordon and D. Sinton, *Anal. Chem.*, 2009, **81**, 4308–4311.
25 J. Zhang and J. Zhu, *Sci. China, Ser. B: Chem.*, 2009, **52**, 815–820.
26 H. Masuda and K. Fukuda, *Science*, 1995, **268**, 1466–1468.
27 D. Berdat, A. Marin, F. Herrera and M. A. M. Gijs, *Sens. Actuators, B*, 2006, **118**, 53–59.
28 I. Vlassiouk, P. Takmakov and S. Smirnov, *Langmuir*, 2005, **21**, 4776–4778.
29 D. Losic, L. Velleman, K. Kant, T. Kumeria, K. Gulati, J. G. Shapter, D. A. Beattie and S. Simovic, *Aust. J. Chem.*, 2011, **64**, 294–301.
30 T. C. Chilcott and C. Guo, *Electrochim. Acta*, 2013, **98**, 274–287.
31 V. V. R. Nandigana and N. R. Aluru, *Electrochim. Acta*, 2013, **105**, 514–523.
32 Z. W. Zhu, Y. Wang, X. Zhang, C. F. Sun, M. G. Li, J.-W. Yan and B. W. Mao, *Langmuir*, 2012, **28**, 14739–14746.
33 J. Feng, J. Liu, B. Wu and G. Wang, *Anal. Chem.*, 2010, **82**, 4520–4528.
34 F. Lisdat and D. Schäfer, *Anal. Bioanal. Chem.*, 2008, **391**, 1555–1567.
35 Z. Siwy and A. Fuliński, *Am. J. Phys.*, 2004, **72**, 567–574.
36 W. Lee, R. Ji, U. Gosele and K. Nielsch, *Nat. Mater.*, 2006, **5**, 741–747.
37 A. M. Md Jani, D. Losic and N. H. Voelcker, *Prog. Mater. Sci.*, 2013, **58**, 636–704.
38 M. C. Zenobi, C. V. Luengo, M. J. Avena and E. H. Rueda, *Spectrochim. Acta, Part A*, 2008, **70**, 270–276.
39 J. Yu, H. Cao and Y. He, *Chemom. Intell. Lab. Syst.*, 2007, **85**, 27–39.
40 P. Takamakov, I. Vlassiouk and S. Smirnov, *Analyst*, 2006, **131**, 1248–1253.
41 A. Girginov, A. Popova, I. Kanazirski and A. Zahariev, *Thin Solid Films*, 2006, **515**, 1548–1551.
42 R. Singh, P. P. Sharma, R. E. Baltus and I. I. Suni, *Sens. Actuators, B*, 2010, **145**, 98–103.